

CHAPTER II

Time-Resolved Extreme-Ultraviolet Photoemission Spectroscopy

In conventional surface analysis, x-ray photoemission spectroscopy (XPS)¹ and ultraviolet photoemission spectroscopy (UPS) are standard methods for analyzing metal surfaces. These methods have proven to be powerful in characterizing metal surfaces, and UPS is especially important for obtaining information about molecules adsorbed on metal surfaces. Photons in the extreme ultraviolet and soft x-ray regimes (50 to 200 eV) are of particular importance in probing metal surfaces. This is due to the fact that the mean free path of photoemitted electrons excited by these photons is extremely short in metals (only about 5 to 10 Å); hence, only electrons originating from the top several mono-layers will be detectable [2]. These photons can be generated using synchrotron radiation or laboratory-size x-ray and ultraviolet light sources.

A long standing goal of chemical physics has been to follow a chemical reaction from beginning to end, while identifying all the intermediate steps. However, conventional UPS techniques are incapable of doing this due to the limitations of the light source used. State-of-the-art – or so called third generation – synchrotrons cannot provide light pulses

¹In chemistry literature, XPS often is referred as Electron Spectroscopy for Chemical Analysis (ESCA).

shorter than tens of picoseconds duration, despite the high photon flux that can be obtained. Since molecular motion (vibrational, rotational, and translational) on metal surfaces is estimated to occur on sub-picosecond time scales, the development of innovative ultrafast light sources that provides EUV pulses with femtosecond duration will provide crucial tools for future investigations.

Several approaches for generating ultrafast EUV light are currently being pursued, including “slicing” synchrotron radiation bunches with femtosecond lasers, Thomson scattering from an electron beam [40, 41, 42], free-electron lasers (FELs) [43, 44, 45], and high harmonic generation techniques. FELs should be capable of generating EUV pulses with sub-picosecond pulse width and extremely high intensity. Practical implementations are still lacking, however, as these technologies are extremely difficult and expensive [46].

A very successful approach to obtaining ultrafast EUV pulses is high harmonic generation. Harmonic generation has a long history – optical frequency doubling was first demonstrated by using a ruby laser and a quartz crystal in 1961 [47]. Since then, techniques for up-converting photons to higher energies have attracted significant attention. In the last decade, the use of harmonic generation for EUV generation has been a topic of extensive investigation, with the demonstration of very high ($> 100^{th}$) order nonlinear processes [48].

2.1 High Harmonic Generation

Ultrafast laser technology has progressed rapidly during the last two decades. In particular, the invention of the ultrafast Ti:Sapphire laser is of great importance [1, 49]. Not only is it an all solid state laser system and therefore relatively easy to use, but furthermore,

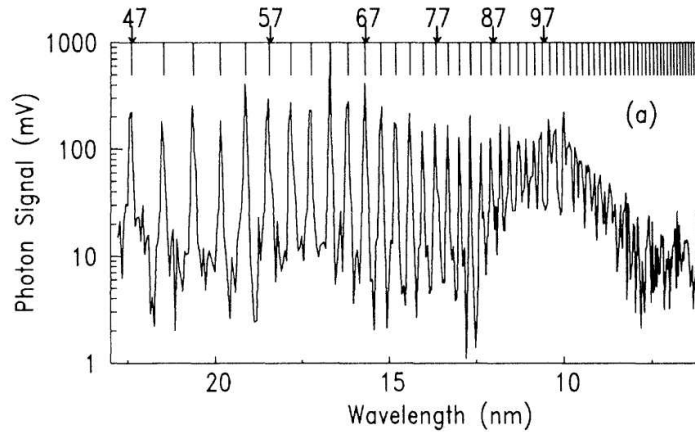


Figure 2.1: High harmonics generated in neon gas at 40 torr with a 1 ps duration, $1.053 \mu\text{m}$ Nd laser pulse at an intensity of $1.5 \times 10^{15} \text{ W/cm}^2$. (figure reproduced from Ref. [50])

the laser pulses generated by Ti:Sapphire oscillators can straightforwardly be amplified using subsequent laser amplifiers. Therefore, table-top size, sub-terawatt class Ti:sapphire laser systems have been constructed and are in use in many laboratories around the world. When these intense laser pulses are focused into a gas medium, the interaction between the strong optical field and the gas atoms produces strong nonlinear-optical effects. One of these effects is the production of optical photons with frequencies corresponding to the odd harmonic orders of the original pulse. The wavelengths of these high harmonic generated (HHG) photons spread across the ultraviolet, the extreme ultraviolet, and the soft x-ray regions of the spectrum. Furthermore, since the high harmonic generation process is a coherent process, the generated photons are highly coherent. This coherent property is important for many physical experiments.

A typical high harmonic generated spectrum produced by an intense ultrafast pulse focused into a noble gas media is shown in Fig. 2.1. The major features of the spectrum are a plateau at low photon energy, and a “cutoff” corresponds to the maximum achiev-

able photon energy. Beyond the cutoff energy, the intensity of the HHG falls rapidly. The emitted spectrum is not continuous, but features discrete harmonic peaks whose energies correspond to the odd harmonic orders of the driving laser. The high harmonic generation process can be explained using a strong field laser-atom interaction model, in which the linearly polarized electric field suppresses the electric field binding electrons to the interacting gas atom [51, 52, 53]. This allows the atom's valence electrons to tunnel out of its attractive potential and into free space, as shown in Fig. 2.2(a). The freed electrons are then accelerated to a very high kinetic energy by the strong electric field of the ultrafast pulse. After a half optical cycle, the ultrafast pulse reverses its electric field, and the electrons are forced to reverse their course. They may then recombine or scatter with the atomic core if their trajectory approaches the parent ion. The high impact energy of this collision causes them to release this kinetic energy into a high energy photon, as shown in Fig. 2.2(b). Since the electrons undergo this process in a very short timespan, the duration of the generated pulses is equally short, on the order of a half cycle of the driving pulse, although the total emission may consist of a train of such pulses. Furthermore, since the electrons from different atomic cores undergo coherent acceleration from the driving pulse, the generated photons are coherent in nature.

Due to the total symmetry of the gas atoms, the generated photons are the odd harmonics of the driving pulse, and extend to the cutoff frequency ω_{max} . Theory predicts a ω_{max} corresponding to the acquired kinetic energy plus the atomic binding energy

$$\hbar\omega_{max} \simeq I_p + 3.2U_p \quad (2.1)$$

where I_p is the ionization potential of the gas atom, and U_p is the cycle-averaged kinetic

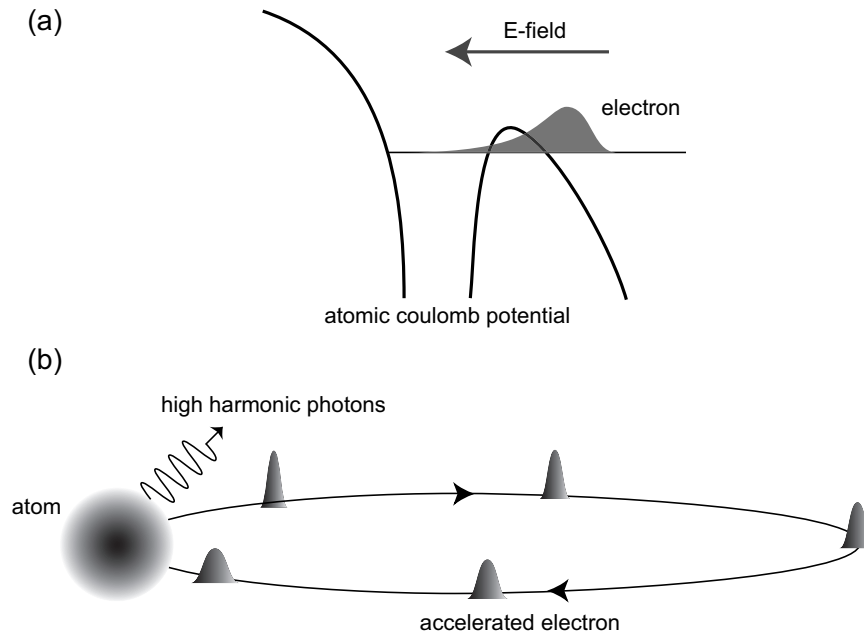


Figure 2.2: In the semi-classical picture, (a) the atomic coulomb potential is disturbed by the laser electric field, and the electron wave packet tunnels through the weakened potential barrier to escape. (b) The electron wave packet enters the free space “continuum” and continue to accelerate in the laser field. On the subsequent half cycle, the electron is decelerated and turns around to be accelerated towards the parent ion. The electron with high kinetic energy then scatters with the parent ion to generate high harmonics.

energy of the electron in an electric field E_0 and frequency ω_0 , generally called the ponderomotive potential. U_p can be written out as

$$U_p = \frac{e^2 E_0^2}{4m\omega_0^2} = \frac{2\pi c r_e I_L}{\omega_0} \quad (2.2)$$

where I_L is the laser field intensity, and $r_e = e^2/4\pi\epsilon_0 mc^2$ is the classical electron radius. To achieve as high a cutoff energy as possible, noble gases, with their higher ionization potentials, are typically used in the high-harmonic generation process. For example, helium's ionization potential is 24.5 eV, and for a laser intensity of 10^{15} W/cm² with a 800 nm wavelength, $\omega_0 = 2.4 \times 10^{15}$ rad/s and $r_e = 2.8 \times 10^{-13}$ cm, so $U_p \simeq 60$ eV. Therefore, using Eq. 2.1, the theoretical maximum generated photon energy is about 220 eV for those conditions. Currently, the record for high harmonic generation is the 229th harmonic (2.7 nm or 450 eV) [3].

To generate “bright” high harmonic pulses, harmonic photons generated at different points in the nonlinear medium have to interfere constructively; otherwise, the generated photons will convert back to the fundamental wavelength. Therefore, extending the medium length does not automatically result in higher output flux. To illustrate this point, for second-order harmonic (2ω) generation in a nonlinear medium, the generated photon intensity can be written as:

$$I_{2\omega} \propto \frac{\sin^2(\Delta k L/2)}{(\Delta k L/2)^2} = \text{sinc}^2\left(\frac{\Delta k L}{2}\right) \quad (2.3)$$

where L is the length of the non-linear media, and

$$\Delta k = 2k_\omega - k_{2\omega} = \frac{2\omega}{c} (n_\omega - n_{2\omega}) \quad (2.4)$$

where k_ω (n_ω) and $k_{2\omega}$ ($n_{2\omega}$) are the wave vector (index of refraction) of the nonlinear medium at wavelengths ω and 2ω , respectively.

Since Eq. 2.3 is a sinc function, it reaches its maximum when $\Delta k = 0$. Therefore, in order to achieve maximum output intensity for a given harmonic, the wave-vectors (2 of k_ω and a $k_{2\omega}$) of the fundamental and harmonic light must cancel out. Eq. 2.4 expresses this “phase-matching” condition for harmonic generation.

For second order harmonic generation, the phase matching condition is easy to achieve, either by temperature-controlling the non-linear medium, or by using a nonlinear crystal and rotating the crystal to the so-called “phase-matching” angle. The idea of both techniques is to achieve equal values for both n_ω and $n_{2\omega}$, in order to satisfy the phase-matching condition. However, phase-matching harmonic generation for high-orders is not so trivial since one cannot use the material birefringence. Furthermore, in the case of HHG, the medium is unavoidably adsorbs much of the generated signal. Therefore, high harmonic generation generally suffers from low output photon flux.

In a typical high harmonic generation setup, a pulsed gas nozzle creates a well-defined region of noble gas inside a vacuum chamber. The gas nozzle pulses synchronously with the incoming focused laser pulses to generate the harmonic light. The reason to use a pulse valve to generate harmonic light is to avoid absorption from the noble gas. However, with such a design it is difficult to achieve high fluxes of the harmonics since harmonic photons are generated in a very limited region with varying pressure.

An innovative design has been implemented in our laboratory using a hollow-core capillary to achieve phase-matching conditions for high harmonic generation. Fig. 2.3

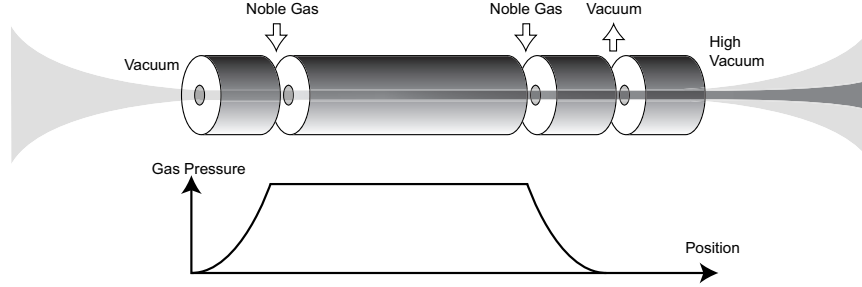


Figure 2.3: Schematic diagram of the hollow-core fiber used to generate the 27^{th} harmonic (42 eV) probe pulse in this experiment. The driving ultrafast beam is drawn in light color and the generated high harmonic beam is in dark color. The fiber has four sections, and the long one is the main harmonic generation region. The noble gas is introduced to the capillary through the gap between the first and second, second and third sections (from the left). The design of having the first and the third short sections sandwiched between the second long section is to maintain a constant pressure at the second section where the high harmonic generation happens. The fourth short section is optionally installed for differential pumping purpose. The inner diameter for all the fibers is $150 \mu m$. The capillary length of all the short sections is 1 cm, and the length for the long section is 8 cm.

shows a schematic illustrating the high-harmonic capillary setup. The long center piece of the hollow core capillary is filled with noble gas. The wave-vector k of the laser beam can be written in the following form when it is traveling inside the capillary [4]

$$k(\lambda) \approx \frac{2\pi}{\lambda} + \frac{2\pi P(1-\eta)\delta(\lambda)}{\lambda} + (1-\eta)n_2I - P\eta N_{atm}r_e\lambda - \frac{u_{11}^2\lambda}{4\pi a^2} \quad (2.5)$$

where the terms, from left to right, correspond to the contributions from vacuum, neutral gas dispersion, non-linear refractive index, plasma dispersion, and waveguide dispersion. The symbols P , η , N_{atm} , $\delta(\lambda)$, r_e , n_2 , I , a and u_{11} represent the pressure in atmospheres, the ionization fraction, the number density at one atmosphere, the neutral gas dispersion, the classical electron radius, the nonlinear refractive index, the laser pulse intensity, the radius of the capillary, and $u_{11} = 2.405$ is the first zero of the Bessel function J_0 . The

important point here is that the wave-vector k depends on the pressure P , driving pulse intensity I , and the capillary radius a ; therefore, the magnitude of the wave-vector k can be controlled by changing these parameters. The phase matching condition for the q^{th} harmonic generation becomes

$$\begin{aligned} \Delta k &= k_q - qk_f \\ &= qk_0 [n(\lambda_q) - n(\lambda_0)] \\ &\approx q \frac{u_{11}^2 \lambda_0}{4\pi a^2} + N_e r_e (q\lambda_0 - \lambda_q) - \frac{2\pi N_a}{\lambda_a} [\delta(\lambda_0) - \delta(\lambda_q)] \end{aligned} \quad (2.6)$$

Therefore, phase-matching for high-harmonic generation can be achieved by “confining” noble gas molecules in a capillary. The high harmonic flux generated in this geometry is estimated to be 10^8 photons/pulse/harmonic at 42 eV in the experimental setup used in this thesis.

One of the favorable properties of the high harmonic source with a hollow-core capillary is that the spatial mode of the generated harmonic beam is rather Gaussian in shape. This allows experimenters to focus the harmonic beam into a small spot size for the investigation of physical phenomena on a microscopic scale (nm in principle), as will be discussed in Sec. 2.2.1. Another desirable property of the high harmonic beam is its spatial and temporal coherence, as pointed out in the previous paragraph. Although UPS generally does not require a coherent source, coherence is a valuable property in many physical investigations. Since pulses generated by synchrotrons are not coherent, high harmonic generation light is not only a convenient replacement of the synchrotron radiation, but unique properties, such as coherence and sub-femtosecond pulse width.

2.2 Time-resolved extreme ultraviolet photoemission spectrometer

The basic method of obtaining time-resolved information of physical phenomena is well understood and has been implemented in a variety of physical investigations. One basic method used to measure physical transients is the “pump-probe” technique. A laser pulse is introduced into the system, which starts a physical process. Another laser pulse is then sent into the system after some time-delay Δt with respect to the first pulse. This second pulse “probes” the status of the system of that moment. Various signals can be measured, including changes of the material reflection and absorption. After probing the system at several time delays and comparing changes among the spectra, a dynamic picture of the physical process is mapped out. Although the idea of pump-probe spectroscopy is simple, measuring the dynamics of surface chemical reactions had not been performed until now. This can now be done by combining two different technologies (UPS and HHG) into one.

The “Time-Resolved extreme Ultraviolet Photoemission Spectrometer” (TR-UPS) that I have constructed is shown in Fig. 2.4. The system consists of two major components – an ultra-high vacuum (UHV) chamber and a pair of IR pump/HHG probe beam lines.

2.2.1 Pump - HHG Probe beam line

As shown in Fig. 2.4, an amplified Ti:sapphire laser system is used as the light source in this experiment. The laser can generate a laser fluence of 1.5 mJ/pulse at a 2 kHz repetition rate. The pulse width is measured to be 22 fs by frequency resolved optical gating (FROG) [54]. The laser beam is directed to a beam splitter, which separates the laser beam into two different pulses – 80% of the laser beam energy will be used as the

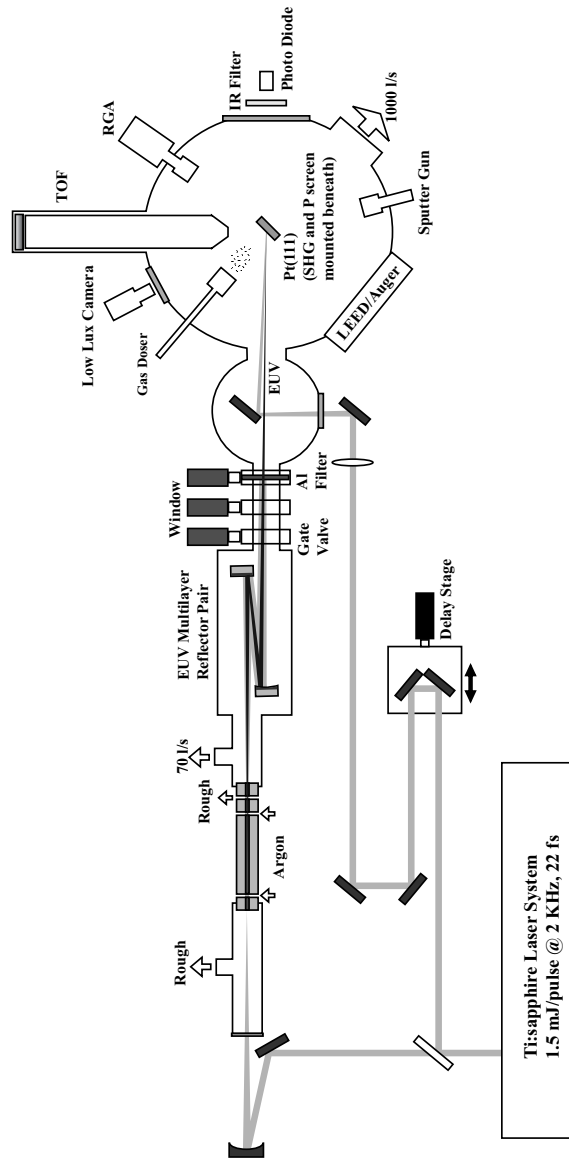


Figure 2.4: Schematic drawing of the time-resolved ultraviolet photoemission spectroscopy. The pump beam is the beam line drawn at the lower part of the figure; the probe beam is drawn at the upper part of the figure, and it goes through the hollow-core capillary to generate high harmonics. The main chamber is under ultra-high vacuum condition at all times ($\sim 10^{-10}$ torr), and a gate valve is used to separate the main chamber from the rest of the system. The multilayer mirror chamber and the beam line are under high vacuum ($\sim 10^{-6}$ torr) condition.

probe, and 20% of the energy becomes the pump. The probe energy will be used for the high harmonic generation process to convert photons in the extreme ultraviolet, and the energy of the resulting EUV pulses will be much less than the energy of the pump beam.

The time delay between the pump and probe beams is varied by using a translation stage in the pump beam. A micro-stepping motor with nanometer step resolution is mounted to the translation stage to give a time delay resolution of better than 1 fs.² The pump beam is then loosely focused into the UHV chamber and subsequently redirected to the sample. The target position of the pump beam on the sample can be readily adjusted by tweaking the mirror mounts outside the vacuum chamber.

For the probe beam, a hollow-core capillary is used to generate high harmonics. Argon gas is used as the nonlinear media for all the experiments discussed in this thesis. The targeted harmonic used in these experiments is the 27th harmonic of the driving 800 nm ultrafast pulses (42 eV in photon energy or 30 nm in optical wavelength). As discussed in Sec. 2.1, harmonic generation produces a semi-continuum spectrum, so frequency discrimination is needed in order to be used in UPS. Traditionally, curved gratings are used for this purpose; however, this scheme suffers from the fact that the reflectivity of the grating of this wavelength is extremely low and the grating itself is difficult and expensive to fabricate. To make matters worse, in order to maintain the sub-picosecond pulse width of the harmonic, two gratings are needed to form a zero-dispersion imaging system [55, 56]. This further reduces the already low reflectivity of the grating spectrometer. In order to avoid this problem, a pair of multi-layer mirrors is used in our setup. This pair of multi-layer mirrors is made by periodically growing silicon and molybdenum thin-films

²The translational stage moves 150 nm to increase or delay 1 fs.

on a super-polished glass substrate to form a Bragg reflector for the incoming EUV photons. The wavelength with the maximum reflectivity is equal to twice the thickness of the Si/Mo stack of the multi-layer mirrors, and the combined reflectivity of the two mirrors is shown in Fig. 2.5. The wavelength of the maximum reflectivity of the multi-layer mirrors is near the 27th harmonic, with a little less than 4% total reflectivity. The adjacent harmonics (25th and 29th) have only 0.5% reflectivity, which effectively filter out these harmonics. The rear multi-layer mirror has a radius of curvature of one meter; hence the multi-layer mirrors also have the benefit of focusing the 27th harmonic onto a small spot of the sample. Fig. 2.6 shows the image of the focal spot of the 27th harmonic. This image is taken by placing a phosphor screen at the sample position, then recording the phosphor fluorescence. The spot size is measured to be 400 μm with a Gaussian profile. The spot size is large because of the long focal length of the curved multi-layer mirror used, and because the sample is not placed exactly at the focal position for convenience. Despite this, the EUV spot size is still small enough for use in photoemission experiments. The infrared pump beam spot size is arranged to be several times bigger than the EUV spot size, to ensure that the probing region of the sample is uniformly illuminated.

A 200 nm thick aluminum filter is inserted between the UHV chamber and the beam line. The transmission of this filter at 42 eV is calculated to be 63% [57]. However, due to the formation of an oxide layer on the surface, the transmission is more typically $\sim 10\%$. The aluminum filter is retracted when the experiment is not running, and a gate valve is shut to separate the beam line from the UHV chamber. The aluminum filter serves two purposes. Firstly, the driving 800 nm pulse is completely reflected by the filter, while the

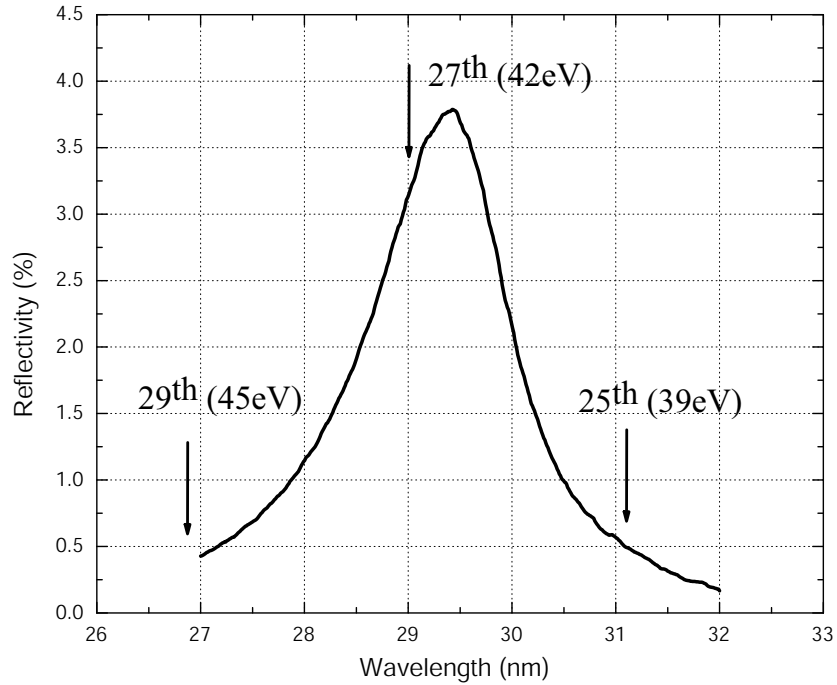


Figure 2.5: Combined reflectivity of the Si/Mo multi-layer mirror pair (2 mirrors) used in the TR-UPS setup. The reflectivity of the mirrors are measured by the synchrotron radiation facility in Lawrence Berkeley laboratory.

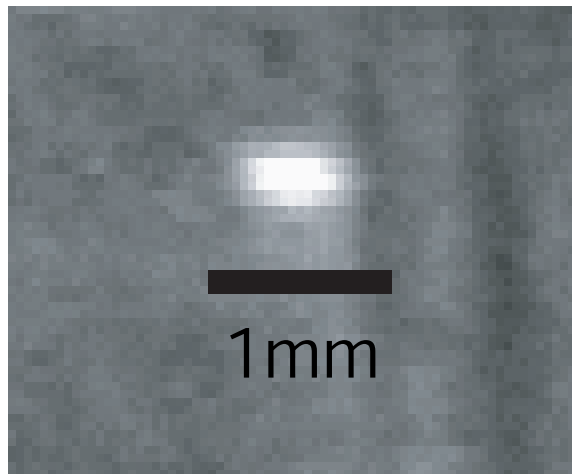


Figure 2.6: The image of the 27th harmonic fluoresce at a phosphor screen. The phosphor screen is mounted beneath the platinum sample, and the phosphor screen was raised to the sample position when this picture was taken. The image was capture by a low-lux, high sensitive camera mounted outside the UHV chamber and looking in through a view port. The spot size of the harmonic is measured to be 400 μm . The spot seems elliptical because the phosphor screen is at 45 degrees with respect to the incoming EUV beam.

harmonics pass through and enter the main chamber. Secondly, the filter is mounted on an air-tight gate valve, which maintains the ultra-high vacuum in the main chamber.

The number of photons that reaches the sample can be calculated using the overall transmission: $10^8 \times 4\% \times 10\% \approx 4 \times 10^5$ photons for the 27th harmonic, with about a 1 eV energy bandwidth.

2.2.2 Ultra-high Vacuum Chamber

The UHV chamber is pumped by a 500 l/s turbo pump (Balzers TMU-520-SG) and a 270 l/s ion pump (Varian VacIon Plus 300 noble diode) to achieve a base vacuum pressure of under 1×10^{-10} torr after a standard UHV bake out. To prevent the earth's magnetic field from penetrating into the vacuum chamber, the chamber is shielded internally by double layers of μ -metal. This prevents the course of photoelectrons from being distorted by external magnetic fields. A platinum(111) single crystal is mounted inside the chamber by spot-welding it onto two parallel tantalum heating wires, which are in turn spot-welded to a manipulator mounted vertically from the top port of the chamber. The manipulator has the capability of performing three-axis translational and azimuthal rotational motion with respect to the platinum sample. In addition, the manipulator's inner tube can be filled with liquid nitrogen, providing cooling of the sample. A high current power supply (HP 6269B) is connected to the manipulator and drives the tantalum wires that heat the platinum sample. A proportional-integral-derivative (PID) temperature controller (Omega CN77000) controls this power supply. A K-type thermocouple is also spot-welded to the back of the platinum sample for measuring the sample's instantaneous temperature. The measured temperature feeds into the PID temperature controller as a feedback signal to control the

high current power supply. Using this feedback control scheme, the electrical heating can be nicely balanced by the liquid nitrogen cooling; therefore, the sample temperature can be reliably controlled over a wide temperature range, from 77 to 1200 K, and the temperature can be increased or decreased at a rapid rate.

A custom-built time-of-flight (TOF) electronic kinetic energy analyzer is used for detection. Two shielding layers of μ -metal are also installed around the inner wall of the TOF tube to insulate it from the earth's magnetic field. The total tube length is $L_{tube} = 600$ mm and the inner diameter is 40 mm, which provides an electron collection solid angle of $S \simeq 2 \times 10^{-3}$ steradians. At the end of the TOF tube, a custom-built large area (40 mm) fast-response detector detects the electrons. A double micro-channel plate (MCP) is used at the front of the detector to obtain the gain necessary to detect single electrons. The MCPs amplify the single electron signal by a secondary electron cascade process to detectable signal levels (~ 100 mV). The detector has timing resolution of about 200 ps. Impedance matching of the whole electron detector allows it to operate with a GHz frequency bandwidth. The key ideas of impedance matching are adapted from the design of A. Stolow [58], and a cone-shape anode design ensures that the fast electronic signal propagates into the coaxial cable with no noticeable reflection. Figure 2.7 shows the output signal when an electron arrives at the detector. The signal has a rise time of less than 1 ns and a pulse width of less than 2 ns. The signal is clean, without noticeable reflection. This is crucial to the detection of multiple incoming electrons. The output signal is subsequently delivered to a high frequency pre-amplifier followed by a constant fraction discriminator (EG&G ORTEC 9327), ensuring that the electron arrival time is independent

of output signal intensity fluctuations. An all solid-state time-to-digital converter (TDC) (ACAM AM-F1) measures the electron flight times, referenced to a start signal from the ultrafast laser system. The real electron flight time is actually referenced to the moment when the EUV pulse arrives at the sample, also the moment when the sample starts to emit electrons. This moment appears on the TOF spectrum as an EUV scattered light peak. This peak is a result of the EUV pulse being scattered/reflected from the sample surface, with the scattered EUV light then triggering the detector. Actually, there is a 2 ns time delay between this EUV peak and the real start time, resulting from the propagation of the EUV light to travel from the sample to the detector. This time difference is neglectable due to the fastest photoelectron needs to take more than 100 ns to reach the detector. By subtracting the time of the EUV “start peak” from the measured flight time, the actual electron kinetic energy E_{kin} can be calculated by the following equation

$$E_{kin} = \frac{1}{2}m_e\left(\frac{L_{tube}}{t_f}\right)^2 \quad (2.7)$$

where m_e is the electron mass, t_f is the subtracted electron flight time.

If the electron emission is assumed to be evenly distributed over the 2π solid angle (half sphere) for rough estimation, the count rate of photoelectron detection C_R (electrons/second) can be calculated using

$$C_R = \frac{S}{2\pi}(1 - R)I \cdot \alpha \cdot D \cdot L_{rep} \quad (2.8)$$

where $S = 2 \times 10^{-3}$ is the solid angle of the TOF, $I = 4 \times 10^5$ is the incoming photon number per pulse, R is the reflectivity of the sample, and $L_{rep} = 2$ kHz is the ultrafast laser repetition rate. $\alpha \simeq 8\%$ is the photoelectric yield of platinum surface at 30 nm [59, 60]. D

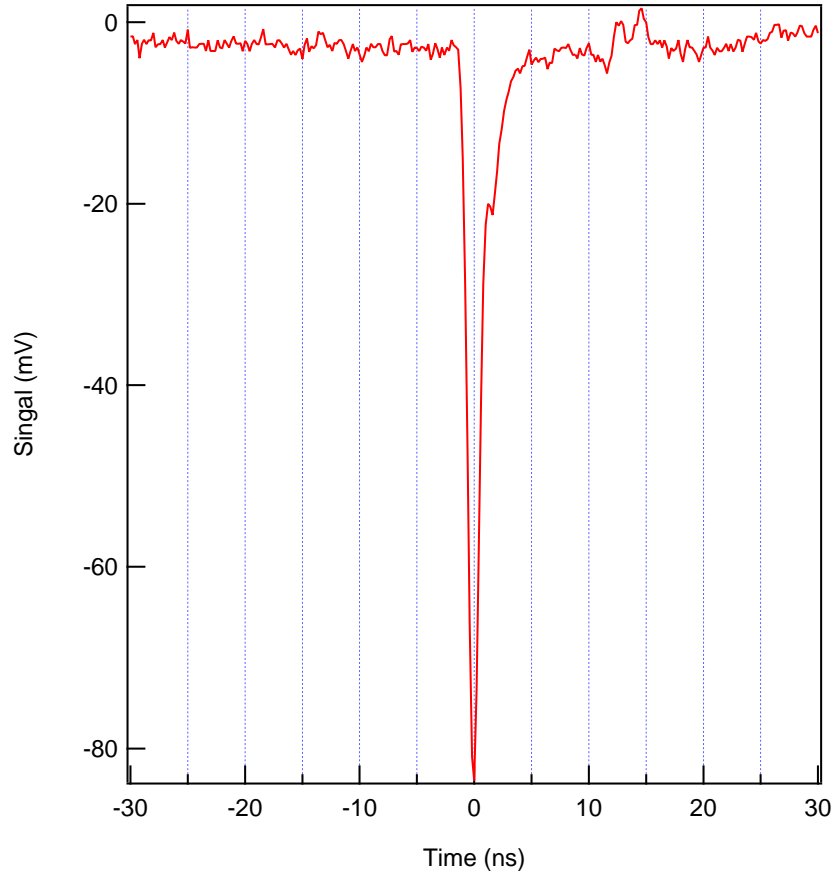


Figure 2.7: The output signal of the impedance matched MCP TOF detector when a single electron hits the detector. The signal is directly measured from the detector with an oscilloscope. It is very important that there is no signal reflection or “ringing” after the main peak for high count rate electron detection.

is the detection efficiency for the MCP detector, and is measured to be $\sim 50 - 85\%$ for the electron kinetic energy range of $0.2 - 2$ keV [61]. For the platinum (111) single crystal, at an incident angle of 45 degrees, $R = 9\%$ [57]. Therefore, the estimated count rate is $C_R \approx 1.5 \times 10^4$ electrons/second, while the experimental count rate is also $C_{Rexp} \approx 1.5 \times 10^4$ electrons/second.

Figure 2.8 shows the inside of the UHV chamber. For standard surface diagnostics, the UHV chamber is equipped with a Low Energy Electron Diffraction (LEED) Spectrometer

and an Auger Electron Spectrometer (AES) (OCI BDL800IR), which monitor the sample surface's condition. The diffraction pattern of the LEED can reveal the local order of the sample surface, while surface contamination can be seen using the AES. A residual gas analyzer (RGA) (Leybold Inficon Transpector) is installed on the UHV chamber for monitoring the ambient chamber gas content. In addition, Thermal Desorption Spectra (TDS) can be taken by the RGA, measuring the partial pressure of a target molecule while the temperature of the sample is steadily raised. A TDS measurement for the O₂/Pt(111) system is shown in Fig. 3.2.

For sample preparation and cleaning, an argon ion sputter gun is installed in the UHV main chamber. The sputter gun can be used to remove the topmost several mono-layers of the platinum sample; sample surface contaminations are simultaneously removed. Rapid thermal annealing can subsequently be performed to reconstruct the surface order.

Finally, a custom-built gas doser is used for precision gas dosing. The major benefit of using a gas doser versus using a gas leak valve is that a doser allows a much higher local pressure to be created around the sample area while keeping the rest of the chamber in high vacuum. This also minimizes the opportunity for gas molecules to adsorb the UHV main chamber wall, preventing prolonged pump down times after gas dosing. In addition, if experimentally required, continuous gas dosing to the sample would not cause serious problems. Maintaining the high vacuum condition of the rest of the system is needed to ensure the functionality of other highly sensitive equipment. For example, the working pressure of the MCP electronic detector must be lower than 1×10^{-6} torr.

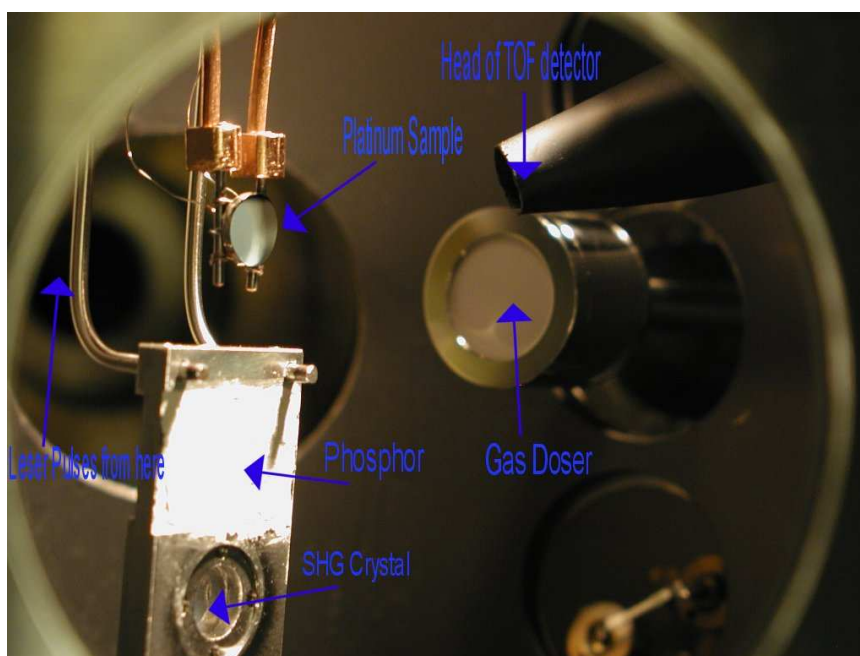


Figure 2.8: Picture shows the internal arrangement of the TR-UPS chamber. In this photo, the sample is turned 90 degrees from the normal position for better viewing. Both of the pump-probe beams are coming in from the flange at the left side of the picture to reach the metal sample.

2.2.3 Finding temporal and spatial overlap

For any pump-probe experiment to be successful, finding the temporal and spatial overlap between the pump and probe beams is critical. In this experiment, the relatively low intensity of the high harmonic generated EUV beam creates a particular alignment challenge. In addition, it is a challenge to find the temporal overlap between an EUV (probe) pulse and an infrared (pump) pulse [62]. Therefore, to routinely run this experiment, an effective method for finding both the temporal and spatial overlap is needed.

To find the temporal overlap, or so-called “time-zero”, some of the infrared light used to create the EUV probe beam is allowed to enter the EUV chamber, by retracting the aluminum filter and inserting a thin sapphire window instead. The argon gas of the high-harmonic cell is turned off to reduce the pressure in the beam line. A KDP (second harmonic) crystal mounted underneath the platinum sample is now raised to the sample position, and the time-zero can then be found by looking for the second harmonic cross-correlation signal between the pump and the probe pulses. Since the aluminum filter is only 200 nm thick, the time difference between the generated EUV pulse and the driving infrared pulse reaching the platinum sample is negligible. The time difference due to the removal of the argon gas is also negligible because of the low pressure (~ 50 torr) and short length (8 cm) of the gas interaction region. However, the time difference induced by inserting a sapphire window to the infrared pulse needs to be accounted for. The thickness of the sapphire window is 355 μm , hence the time delay induced by the sapphire can be precisely calculated to be 934 fs. This time difference can be corrected for by moving the translational stage after the cross-correlation is found. Therefore, it is effective to find the

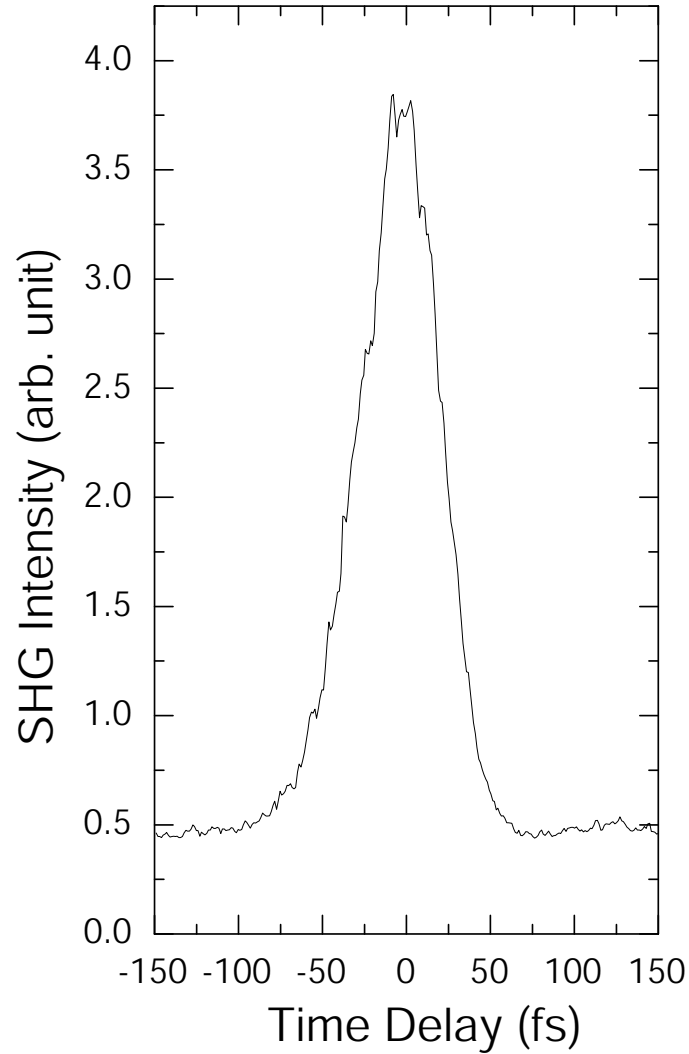


Figure 2.9: Signal of second harmonic generation between the infrared pump and probe pulses. The FWHM of the signal is 62 fs.

time-zero between the probe and pump beam without directly using the EUV pulses. A typical cross-correlation signal for the two beams is shown in Fig. 2.9.

To find the spatial overlap, a phosphor screen (P1 phosphor) mounted beneath the sample is raised to the sample position. The focused EUV spot can be imaged by a highly sensitive, low-lux CCD camera (Minitron 12V1E) mounted outside the chamber. The camera views the phosphorescence through a view port, as shown in Fig. 2.6. Since the

beam pointing of the EUV is fixed and cannot be adjusted, spatial overlap is achieved by moving the infrared pump beam location by adjusting the mirror mounts outside of the chamber. Once the spatial overlap is found, the sample is lowered back to its original position.

2.3 Conclusion

In this chapter, the implementation of the TR-UPS setup was thoroughly discussed and explained. In the following two chapters, the setup will be utilized to measure chemical dynamics of adsorbates on metal surfaces, demonstrating the power of the TR-UPS technique.